



Outdoor-to-Indoor 28 GHz Wireless Measurements in Manhattan: Path Loss, Location Impacts, and 90% Coverage

Manav Kohli¹, Abhishek Adhikari¹, Gulnur Avci¹, Sienna Brent¹, Jared Moser², Sabbir Hossain³, Aditya Dash¹, Igor Kadota¹, Rodolfo Feick⁴, Dmitry Chizhik⁵, Jinfeng Du⁵, Reinaldo A. Valenzuela⁵, Gil Zussman¹

¹Columbia University, ²Stuyvesant H.S., ³City College of New York, ⁴Universidad Técnica Federico Santa María, ⁵Nokia Bell Labs
{mpk2138, aa4832, gza2102, scb2197, add2162, ik2496, gz2136}@columbia.edu, jmoser20@stuy.edu, shossai009@citymail.cuny.edu,
rodolfo.feick@usm.cl, {dmitry.chizhik, jinfeng.du, reinaldo.valenzuela}@nokia-bell-labs.com

ABSTRACT

Outdoor-to-indoor (OtI) signal propagation further challenges link budgets at millimeter-wave (mmWave). To gain insight into OtI mmWave at 28 GHz, we conducted an extensive measurement campaign consisting of over 2,000 link measurements in West Harlem, New York City, covering seven highly diverse buildings. A path loss model constructed over all links shows an average of 30 dB excess loss over free space at distances beyond 50 m. We find the type of glass to be the dominant factor in OtI loss, with 20 dB observed difference between clustered scenarios with low- and high-loss glass. Other factors, such as difference in floor height, are found to have an impact between 5–10 dB. We show that for urban buildings with high-loss glass, OtI data rates up to 400 Mb/s are supported for 90% of indoor users by a base station (BS) up to 49 m away. For buildings with low-loss glass, such as our case study covering multiple classrooms of a public school, data rates over 2.8/1.4 Gb/s are possible from a BS 68/175 m away when a line-of-sight path is available. We expect these results to be useful for the deployment of OtI mmWave networks in dense urban environments and the development of scheduling and beam management algorithms.

CCS CONCEPTS

- General and reference → Measurement; • Networks → Network measurement; Wireless access networks; Physical links.

KEYWORDS

28 GHz; millimeter-wave; urban; channel measurements; path gain models; indoor coverage; material dependence; signal-to-noise ratio

ACM Reference Format:

Manav Kohli¹, Abhishek Adhikari¹, Gulnur Avci¹, Sienna Brent¹, Jared Moser², Sabbir Hossain³, Aditya Dash¹, Igor Kadota¹, Rodolfo Feick⁴, Dmitry Chizhik⁵, Jinfeng Du⁵, Reinaldo A. Valenzuela⁵, Gil Zussman¹. 2022. Outdoor-to-Indoor 28 GHz Wireless Measurements in Manhattan: Path Loss, Location Impacts, and 90% Coverage. In *The Twenty-third International Symposium on Theory, Algorithmic Foundations, and Protocol Design for Mobile Networks and Mobile Computing (MobiHoc '22), October 17–20, 2022, Seoul, Republic of Korea*. ACM, New York, NY, USA, 10 pages. <https://doi.org/10.1145/3492866.3549728>

Permission to make digital or hard copies of all or part of this work for personal or classroom use is granted without fee provided that copies are not made or distributed for profit or commercial advantage and that copies bear this notice and the full citation on the first page. Copyrights for components of this work owned by others than the author(s) must be honored. Abstracting with credit is permitted. To copy otherwise, or republish, to post on servers or to redistribute to lists, requires prior specific permission and/or a fee. Request permissions from permissions@acm.org.

MobiHoc '22, October 17–20, 2022, Seoul, Republic of Korea

© 2022 Copyright held by the owner/author(s). Publication rights licensed to ACM. ACM ISBN 978-1-4503-9165-8/22/10...\$15.00
<https://doi.org/10.1145/3492866.3549728>

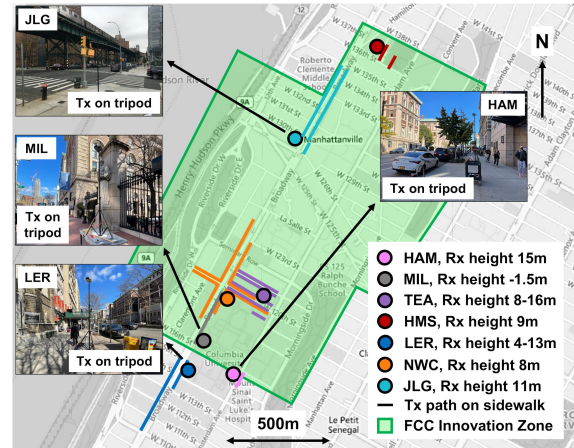


Figure 1: Buildings and corresponding sidewalks where over 2,000 link measurements were collected in and around the COSMOS FCC Innovation Zone in West Harlem, NYC (more details are in Tables 2 and 3, and Figure 2).

1 INTRODUCTION

Millimeter-wave (mmWave) wireless is a key enabler of 5G-and-beyond networks. Its high-throughput potential makes it particularly viable in novel network solutions, such as fixed wireless access (FWA) for providing Internet connectivity to public schools and public housing, helping to bridge the digital divide [1, 2]. A major challenge in using mmWave links, particularly in dense urban environments, is their high path loss, exacerbated in outdoor-to-indoor (OtI) scenarios. In order to guide the development of algorithms (e.g., for beam management [3–5] or link scheduling [6, 7]) and to support deployments (including for indoor coverage by FWA), measurement-based models are needed.

However, while outdoor-to-outdoor (OtO) and indoor-to-indoor (ItI) propagation scenarios have been extensively measured [8–25], existing OtI datasets are relatively small in size [10–12, 26–29]. In this paper we present the results of an extensive OtI mmWave measurement campaign that we conducted in a dense urban environment.

Measurements: As illustrated in Figure 1, we conducted a large-scale measurement campaign in and around the COSMOS FCC Innovation Zone in West Harlem, New York City (NYC) [30, 31]. Using a 28 GHz channel sounder [14], we collected over 2,000 OtI measurements (comprising over 29 million individual power measurements) across 39 OtI scenarios in seven very diverse buildings, covering a variety of construction materials and building utility.

Models: We develop path gain models for each OtI scenario using a single-slope exponent fit to the measured data as a function of distance, and record the CDF of the measured azimuth beamforming

Table 1: Overview of prior ItI, OtO, and OtI measurement studies in urban or suburban environments using various frequency ranges and equipment designs.

Ref.	Type	Frequency	Environment	Tx Design	Rx Design	Bandwidth	# Tx-Rx Links
[8]	ItI	28 GHz	Urban	Stationary Horn	Rotating Horn	Narrowband	>1,500
[9]	ItI, OtO	29 & 60 GHz	Urban & Suburban	Rotating Horn	Rotating Horn	200 MHz	785
[10]	ItI, OtO, OtI	28 GHz	Suburban	Stationary Horn	Stationary Horn	2 GHz	153
[11]	ItI, OtI	60 GHz	Urban	8x1 MIMO Array	8x2 MIMO Array	4 GHz	150
[12]	ItI, OtI	28 GHz	Urban	Gimbal-mounted Horn	Gimbal-mounted Horn	400 Mcps	18
[13]	OtO	60 GHz	Urban	36x8 Phased Array	36x8 Phased Array	2.16 GHz	15
[14]	OtO	28 GHz	Suburban	Stationary Horn	Rotating Horn	Narrowband	>2,000
[15]	OtO	28 GHz	Urban	Omnidirectional	Rotating Horn	Narrowband	>1,500
[26]	OtI	60 GHz	Urban	Stationary Horn	Stationary Horn	125 MHz	76
[27]	OtI	60 GHz	Suburban	Omnidirectional	Rotating Horn	Narrowband	160
[28]	OtI	28 GHz	Urban	8x2 Phased Array	8x2 Phased Array	400 MHz	29
[29]	OtI	28 GHz	Suburban	Stationary Slot Array	Stationary Parabolic Dish	50 MHz	43
<i>This work</i>	OtI	28 GHz	Urban	Omnidirectional	Rotating Horn	Narrowband	>2,000

(BF) gain. We also develop clustered models covering scenarios at each building, and aggregate models to study specific effects: (i) the type of glass used for the windows (low- or high-loss glass), (ii) base station (BS) antenna placement in front of or behind an elevated subway track, (iii) user equipment (UE) placement on upper/lower floors of the building, and (iv) the angle of incidence (AoI) of the mmWave signal into the building. Using these clusters, we show a 20 dB additional loss for the high-loss glass compared to low-loss glass, and a 5–10 dB difference for the other effects.

Case Study - Public School: We consider the Hamilton Grange public school in West Harlem as a case study and provide an in-depth discussion of the OtI scenarios studied there. The low path loss observed in this building along with its location in an area with below-average Internet access make it of particular interest for mmWave OtI coverage via FWA [2]. The dataset obtained for this case study is available at [32].

Multi-User Support: We evaluate multi-user support with two OtI scenarios in a classroom building using typical BS placements on building edges. For indoor users located far from the BS, we find that inter-user-interference (IUI) can be significant, with a median correlation coefficient of 0.79 between the directions of received power at the BS. This could hamper the BS' ability to serve multiple users with multiple beams. IUI is reduced when the BS is located closer to users and a wider range of angles are available.

Coverage: We calculate achievable data rates for an indoor UE using the path gain models for low-loss and high-loss glass. We show that data rates in excess of 2.8/1.4 Gb/s are possible in low-loss glass OtI scenarios for up to 90% of users with the BS up to 68/175 m away. For high-loss glass OtI scenarios, we find achievable data rates in excess of 400 Mb/s for BS placements up to 49 m away.

The rest of the paper is organized as follows. In Section 2, we discuss related work. In Section 3, we describe the measurement campaign, including equipment, locations, and method. In Section 4, we develop path gain models from the measurement data. In Section 5, we focus on the public school case study. In Section 6 we discuss the potential of multi-user support in OtI scenarios, and in Section 7 we derive achievable data rates. Finally, we conclude and discuss future work in Section 8. Additional results can be found in our technical report [33].

2 RELATED WORK

Table 1 provides an overview of a subset of prior efforts. As seen in the table, mmWave measurement studies typically require the use of specialized channel sounders and may be further categorized

based on the type: OtO [9, 10, 13–15, 17–23, 25], ItI [8–12, 16, 17, 20, 24, 25], and OtI [10–12, 26, 28, 29], as well as the frequency range and urban or suburban environment. Datasets that include outcomes of some of these studies are available in [25].

OtO measurements have focused on a variety of environments, including urban [10, 15], suburban [10, 14], and rural [34] mmWave deployment scenarios. Conversely, ItI measurements have primarily focused on one building type: offices [8, 11, 12, 24].

Previous OtI measurements include those at a regional airport [10] and measurements of office space using a receiver (Rx) mounted on a robot and a stationary transmitter (Tx) [11]. Other forms of Tx/Rx mounting have been used, such as a Tx mounted on a van with indoors Rx [26]. Phased array antennas have also been used at the Tx and Rx [28], with 90° beamsteering capability and 5° resolution. Longer-term measurements have also been studied, including a four-day measurement with the indoor Rx and outdoor Tx both kept stationary [29]. Finally, 28 GHz OtI measurements have been collected at small-scale in NYC using a fixed Tx and Rx [12].

While some OtI measurements are available, to the best of our knowledge (and as can be seen in Table 1), this paper is the *first large-scale, measurement-driven study of the OtI mmWave channel in a dense urban environment, leading to reliable statistical models for the path loss and beamforming gain degradation as well as quantitative insights for indoor propagation paths and realistic data rates*.

3 MEASUREMENT CAMPAIGN

In this section, we describe the measurement locations, equipment, and scenarios in the OtI measurement campaign.

Locations: Figure 1 and Table 2 show seven buildings where measurements were conducted. These buildings are located in and around the FCC Innovation Zone [30] associated with the NSF PAWR COSMOS testbed [31] in West Harlem, NYC. In Figure 1, the locations of these buildings are shown along with the corresponding outdoor sites (sidewalks, parking lot, and basketball court). Photos of these buildings are shown as insets in Figure 1 and in Figure 2. Table 3 lists the OtI scenarios for the seven buildings.

In particular, **HAM** and **MIL** are similar buildings located on the corners of two different T-intersections. **HAM** is a classroom building, and **MIL** houses a theater. **TEA** is a large classroom and office building occupying an entire block, which used to house an elementary school. **HMS** is typical inner city public middle school building. **LER** is a more modern building which serves as a student center and overlooks a parallel street. Unlike the older buildings, laboratory buildings **NWC** and **JLG** have a very modern glass

Table 2: Measurement locations considered, as shown in Figures 1 and 2. Corresponding OI scenarios are in Table 3.

Building Name	Abbreviation	Purpose	Year	Construction	Glass Type
Hamilton Hall	HAM	Classroom Building	1907	Brick & concrete	Low-e / High-loss
Miller Theatre	MIL	Theater	1918	Brick & concrete	Low-e / High-loss
Teachers' College	TEA	Classroom and Office Building	1924	Brick & concrete	Low-e / High-loss
M209 Hamilton Grange Middle School	HMS	Public School	1928	Brick & concrete	Traditional / Low-loss
Lerner Hall	LER	Student Center	1999	Brick & concrete	Low-e / High-loss
Northwest Corner Building	NWC	Laboratory Building	2008	Glass, metal, stone	Low-e / High-loss
Jerome L. Greene Science Center	JLG	Laboratory Building	2017	Glass & metal	Low-e / High-loss

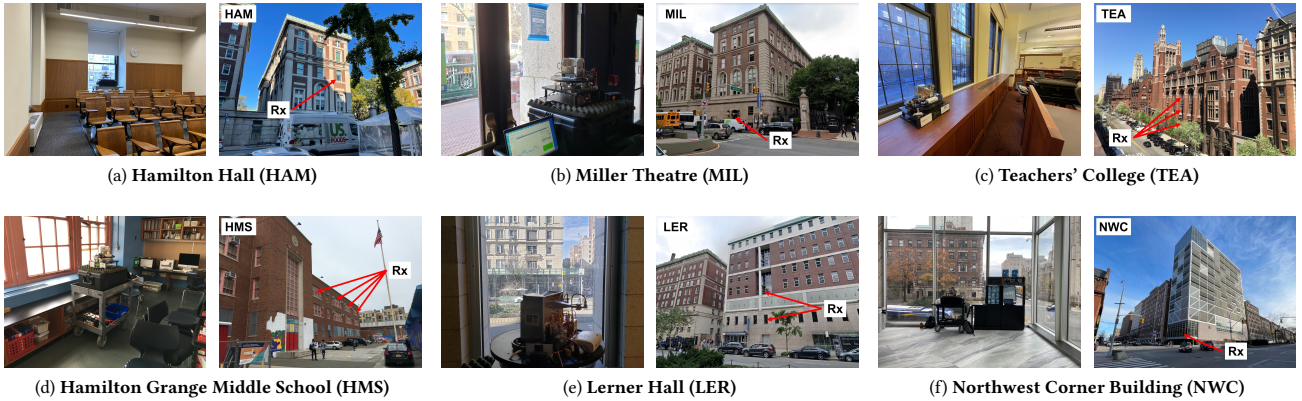


Figure 2: Representative interior and exterior views of six of the seven locations (shown in Figure 1 and Table 2). Rx locations indicated on exterior views.

and metal construction with floor-to-ceiling windows. NWC is located at a four-way intersection, while JLG is located adjacent to a main road with a raised subway track blocking view of the far side of the street. These locations represent a diverse set of building constructions and surrounds that are typical of a dense urban area. **Equipment:** We utilize a 28 GHz channel sounder consisting of a separate Tx and Rx, which is described in detail in [14, 15]. The Tx is equipped with an omnidirectional antenna with 0 dBi gain, and transmits a +22 dBm continuous-wave tone. The Rx is fed by a 24 dBi rotating horn antenna (14.5 dBi in azimuth) with 10° 3 dB beamwidth. The antenna feeds a mixer which downconverts the received signal to 10 MHz intermediate frequency (IF). The IF signal is then passed through two switchable low-noise amplifiers (LNAs) and a bandpass filter. Finally, the IF signal's power is recorded by a power meter with 20 kHz bandwidth and 5 dB noise figure.

Scenarios: For the scenarios in Table 3, we placed the rotating Rx indoors (emulating a UE) and the omnidirectional Tx outdoors (emulating a BS). The Tx was moved along a linear path, such as a sidewalk, at a height of 3.4 m. This emulates lightpole deployments of mmWave BSes along streets, which are slated for widespread use in NYC and other urban areas [35, 36].

A total of 39 scenarios are listed in Tables 3 and 4. For the measurements in Table 3, an OI scenario is defined by the indoor Rx placement within a given building and the outdoors Tx path. In each scenario, we placed the Tx at set intervals along the path whose length is defined by the “Range” column in Table 3. At each such location (namely, every interval), we measured a link to the indoor Rx. The number of links for each scenario is listed in Table 3. For each link measurement, the rotating Rx measured the channel for 20 seconds, corresponding to 40 full rotations at 120 RPM. A power reading was taken 740 times per second, providing at least 14,800 power readings per link measurement.

Using the same equipment but in different setups, four additional OI scenarios were studied, which are listed in Table 4. The first

and second, detailed in Section 5.2, investigate the path loss and signal propagation within an interior hallway at HMS. The Tx was kept stationary outdoors and the Rx moved indoors. The third and fourth, detailed in Section 6, investigate the potential of supporting multiple users, a consideration for multi-user MIMO systems. The Rx was kept stationary outdoors and the Tx moved indoors. *In total, we took over 2,000 Tx-Rx link measurements representing over 29 million individual power measurements.*

4 MEASUREMENT RESULTS

In this section, we use the data obtained from the measurement campaign to develop path gain models for the 35 OI scenarios covered in Figure 1 and Table 3. Each scenario name in Table 3 is structured as LOC-X-Y-#, where LOC is a location in Figure 1, X is the cardinal direction of the Tx relative to the Rx, Y is the sidewalk along which the Tx was moved, and # is the floor of the building in which the Rx was placed, if applicable. In some OI scenarios at TEA, the Tx was moved along an outdoors balcony on the opposite side of the street instead, indicated by “Bal”. The measurements at HMS use a different naming scheme. The first value refers to the Tx path that was used (along a parking lot or along a basketball court) and the number refers to the classroom where the Rx was.

The path gain models in Table 3 show large differences even for OI scenarios at the same building, for example the measurements JLG-E-E¹ and JLG-N-E. This means very few conclusions can be drawn from individual scenarios. We can develop better insight by clustering OI scenarios in certain ways. We first cluster the OI scenarios by building, as seen in Figure 3. We compute a path gain model for each building, along with distributions of the azimuth beamforming gain and temporal k-factor. Significant differences between buildings with outwardly similar appearances are found.

¹The very high positive slope is due to a small measurement range at a comparatively large offset from the building.

Table 3: 35 OI measurement scenarios with computed path gain model and median azimuth beamforming gain.

Name	Color	Group	Range (m)	Step (m)	# Links	Slope (dB)	Intercept (dB)	RMS (dB)	Median G_{az} (dBi)
HAM-S-E	Pink	HAM	61	1	62	-6.61	-23.7	3.5	11.1
MIL-N-E	Gray	MIL	155	2.5	76	-3.53	-59.1	2.8	11.0
TEA-S-N-1	Purple	TEA	230	6/8	35	-2.56	-95.3	5.6	11.0
TEA-S-S-1	Purple	TEA	228	4/8	45	-3.49	-75.1	4.8	10.9
TEA-S-S-2	Purple	TEA	155	3	52	-5.52	-40.5	2.6	7.7
TEA-S-S-3	Purple	TEA	232	3	77	-5.13	-36.1	3.3	8.8
TEA-S-Bal-1	Purple	TEA	85	3	29	-1.61	-107.9	4.7	9.7
TEA-S-Bal-2	Purple	TEA	85	3	29	-0.69	-111.3	4.2	7.8
TEA-S-Bal-3	Purple	TEA	37	3	13	-5.20	-33.6	4.3	10.0
TEA-N-N	Purple	TEA	243	3	68	-4.45	-53.0	4.1	10.8
TEA-N-S	Purple	TEA	243	3	81	-4.80	-41.0	4.1	10.1
HMS-Lot-307	Maroon	HMS	62	1	63	-3.22	-60.4	1.6	10.4
HMS-Lot-317	Maroon	HMS	62	1	63	-3.48	-52.0	3.4	11.5
HMS-Lot-321	Maroon	HMS	62	1	63	-4.12	-44.1	3.4	11.8
HMS-Lot-323	Maroon	HMS	62	1	63	-4.10	-47.2	2.5	9.9
HMS-Lot-325	Maroon	HMS	62	3	22	-3.40	-54.8	2.5	10.8
HMS-Court-307	Maroon	HMS	42	1	43	-5.47	-3.9	2.9	13.3
HMS-Court-317	Maroon	HMS	39	1	40	-6.48	11.2	3.2	12.0
HMS-Court-321	Maroon	HMS	57	1	58	-8.50	51.1	3.1	11.0
HMS-Court-323	Maroon	HMS	57	1	58	-8.13	43.6	1.6	9.8
HMS-Court-325	Maroon	HMS	58	1	59	-1.88	-84.3	2.2	10.2
LER-S-W-5	Blue	LER	298	3	96	-5.29	-19.6	3.0	10.8
LER-S-W-2	Blue	LER	110	8	14	-6.72	-22.8	4.2	9.4
LER-S-E-2	Blue	LER	95	6	23	-3.97	-75.2	3.8	9.4
NWC-N-W	Orange	NWC	197	3/6	65	-3.03	-76.9	4.7	12.8
NWC-N-E	Orange	NWC	201	3	60	-3.52	-73.0	1.9	11.2
NWC-E-N	Orange	NWC	131	3	44	-4.83	-48.7	2.9	11.1
NWC-E-S	Orange	NWC	242	3	78	-3.08	-83.2	2.8	10.8
NWC-S-E	Orange	NWC	105	1	106	-3.30	-86.7	4.9	9.8
NWC-S-W	Orange	NWC	180	2/3/6	72	-3.36	-74.9	4.5	10.9
NWC-S-E	Orange	NWC	153	3	46	-4.36	-55.4	4.2	12.1
NWC-W-N	Orange	NWC	173	3	56	-2.02	-102.4	3.2	10.3
JLG-N-W	Cyan	JLG	291	3/6	75	-2.94	-72.5	2.5	10.8
JLG-N-E	Cyan	JLG	224	3	68	-3.20	-77.7	2.3	8.9
JLG-E-E	Cyan	JLG	49	3	17	11.61	-355.6	2.9	13.1

Table 4: Four additional OI measurement scenarios with different Tx and Rx locations

Name	Group	Range (m)	# Links	Tx & Rx placement	Purpose
HMS-Lot-Hallway	HMS	57	58	Tx stationary outdoors, Rx moved inside	Studying signal loss and propagation further indoors (§5.2)
HMS-Court-Hallway	HMS	57	58	Tx stationary outdoors, Rx moved inside	Studying signal loss and propagation further indoors (§5.2)
TEA-S-Corner-1-Reverse	TEA	230	17	Rx stationary outdoors, Tx moved inside	Evaluating multi-user coverage potential (§6)
TEA-S-Middle-1-Reverse	TEA	111	19	Rx stationary outdoors, Tx moved inside	Evaluating multi-user coverage potential (§6)

We then cluster OI scenarios in Figures 4(a) and 5 based on the type of window glass: “traditional” or low-emissivity (Low-e). We also compare the measurement data to OI models derived from 3GPP models for path loss and building penetration loss in Figure 4(b). We then consider several Tx-Rx placements: (i) Tx behind/in front of an elevated subway track, (ii) Rx on different floors of the same building, and (iii) angle of incidence (AoI) less/greater than 45° into the window near the Rx with results in Figure 6.

4.1 Measurable Parameters

Four parameters are calculated from the data: (i) path gain, $G_{path}(d)$, (ii) azimuth angular spectra of the received power $\bar{S}(d, \phi)$, (iii) effective azimuth beamforming gain $G_{az}(d)$, representing the effect of angular spread, and (iv) the temporal k -factor $K(d)$, representing the time-varying component of the channel, such as the movement of cars, pedestrians, etc., as a fraction of the total signal power. In [33], we provide additional details on how these values are derived.

$G_{path}(d)$ and $G_{az}(d)$ are important parameters as they will define the signal-to-noise ratio (SNR) of a Tx-Rx link; we use the SNR to study the achievable data rates in Section 7. Any $G_{az}(d)$ below the nominal value of 14.5 dBi indicates beamforming gain degradation resulting from environmental scattering. We use $\bar{S}(d, \phi)$ to

understand OI propagation paths in Section 5.2 and multi-user MIMO support in Section 6.

4.2 Different Buildings

Figure 3 shows the measured path gain, azimuth beamforming gain, and temporal k -factor for all building clusters. The best-fit path gain models for each building are also displayed in Figure 3(a).

Most notably, Figure 3(a) shows that **HMS** experiences path gain 10–25dB higher than other buildings at 50 m three-dimensional Euclidean distance between Tx and Rx. Figure 3(b) shows that the median azimuth beamforming gain for all buildings are within 1.2 dB of each other, an inconsequential difference overall, though we note that buildings with larger windows (**TEA**, **NWC**, and **JLG**) tend to have lower azimuth beamforming gain than others. This is likely due to the larger windows permitting signal penetration from more directions. Figure 3(c) shows that the median temporal k -factor can vary by around 8 dB, which is primarily due to different time-varying outdoor environments at each building.

The large differences in Figure 3(a) between buildings of similar construction (for example, **HAM** and **MIL** in Figure 2) suggest that construction alone is not a good indicator of the expected loss.

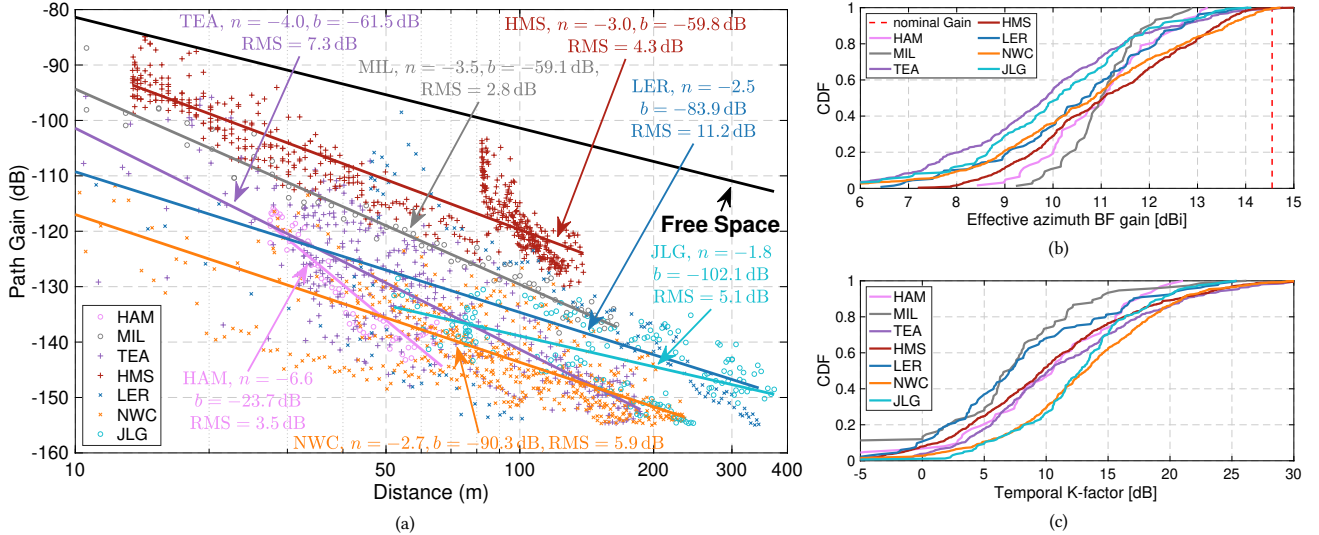


Figure 3: Measurement results clustered by building: (a) average path gain as a function of the 3-dimensional Tx-Rx link distance, with models for each building plotted and noted, (b) CDF of azimuth beamforming gain, (c) CDF of temporal k -factor.

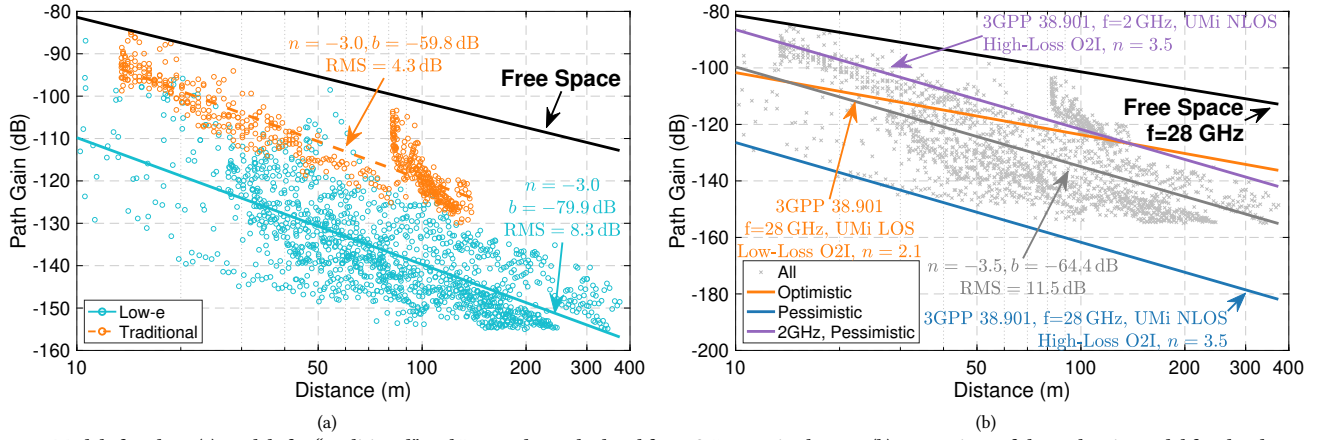


Figure 4: Models for glass: (a) models for “traditional” and Low-e glass calculated from O2I scenario clusters, (b) comparison of the path gain model for the cluster of all O2I scenarios to optimistic and pessimistic models developed from 3GPP UMi path loss predictions for different types of glass.

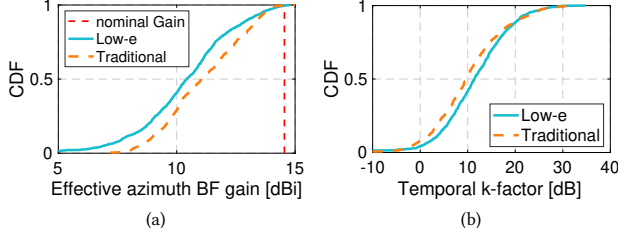


Figure 5: Measurement results categorized by the type of glass used. CDFs of (a) effective azimuth beamforming gain and (b) temporal k -factor

4.3 Low-e and Traditional Glass

4.3.1 Measurements. In order to understand the specific factors that may impact the path loss for a building, we first group the measurements based on the type of glass. “Traditional” glass, often used in buildings predating the availability of float glass in the 1960s, typically has less than 1 dB loss at 28 GHz [37]. Modern Low-e glass can have losses in excess of 25 dB [38]; we measured a loss of 40 dB at normal incidence from the Low-e glass at NWC [33]. Loss as high as 50 dB through concrete walls at 28 GHz [39] implies that

the majority of the mmWave signal will be received via windows, suggesting them to be a significant factor impacting path loss.

HMS uses “traditional” glass, while the other six locations use Low-e glass in their construction; the windows at older buildings have been reglazed in recent years. The results of this analysis are presented in Figures 4 and 5. The path gain models for both categories are shown in Figure 4(a). We observe that the models have identical slopes, with the difference being a uniform 20 dB additional loss experienced by the buildings with Low-e glass.

The results for the azimuth beamforming gain and temporal k -factor are shown in Figures 5(a) and 5(b). These two quantities are very similar, with an azimuth beamforming gain degradation of 3.5–4.5 dB and median k -factor value of 10–12 dB. This is to be expected, as these values are influenced primarily by the overall measurement environment rather than by the type of glass. The results indicate a moderate level of beamforming gain degradation and reasonable channel stability over time; the median temporal k -factor is 10 dB, indicating that the time-varying component of the received signal is one-tenth of the total power.

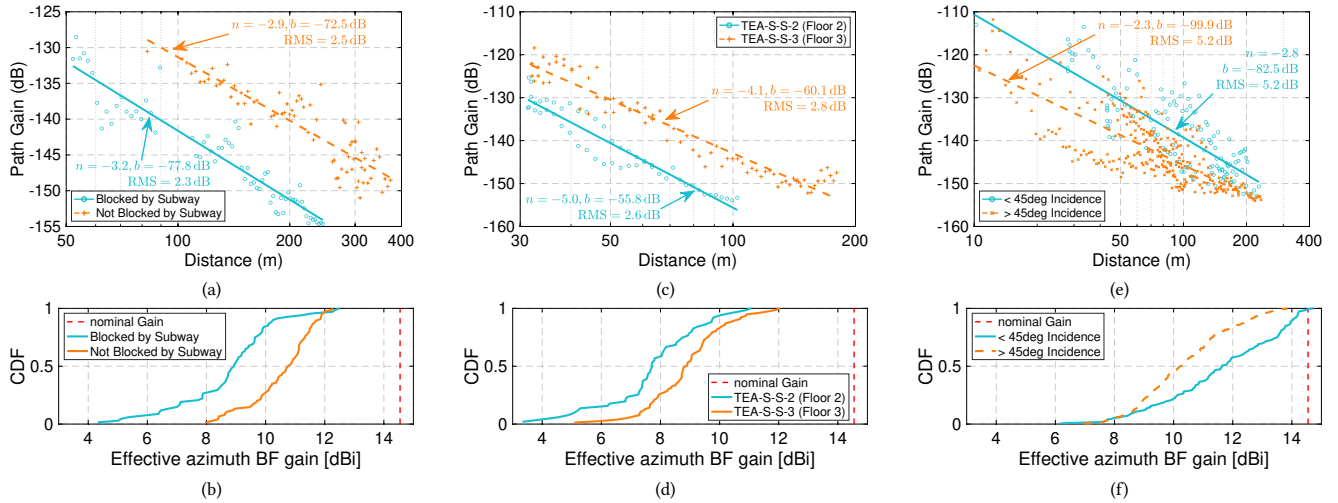


Figure 6: Path gain and azimuth beamforming gain measurements for different placements of Tx and Rx: (a,b) Tx placed on different sides of the same street measured from JLG, (c,d) Rx placed on different floors of TEA, and (e,f) AoI above or below 45° at NWC.

4.3.2 Comparison to 3GPP Predictive Models. Figure 4(b) shows a path loss (PL) model aggregated over all Oti scenarios in Table 3 compared to pessimistic and optimistic models developed from 3GPP TR 38.901 [40]. The pessimistic model is defined as $PL_{pess}(d) = PL_{Oto,NLOS}(d) + PL_{Oti,High}$, which is the sum of the non-line-of-sight (NLOS) urban street canyon model (USCM) and building transmission loss with Low-e glass. We use the NLOS model for two reasons. First, beyond 52 m, the 3GPP NLOS probability will exceed 50% [40], and the majority of our measurement data is at distances larger than 52 m and thus prone to occlusion by trees and other sidewalk clutter. Second, this model can provide an upper bound for the expected path loss. Similarly, to give a lower bound on the expected path loss, the optimistic model is defined as $PL_{opt}(d) = PL_{Oto,LOS}(d) + PL_{Oti,Low}$, using the LOS USCM and building transmission loss with “traditional” multi-pane glass. In addition, a pessimistic model at 2 GHz is included in the figure. In all models we set the BS height to 10 m and the UE height to 3.5 m.

The 35 Oti scenario measurements predominantly fall between the two 28 GHz models. There are a number of points which lie above the optimistic line; these are mostly from **HMS**. This is largely due to the single-pane “traditional” glass windows, which should produce even less building transmission loss than predicted by $PL_{Oti,Low}$. The tendency for the measured path gain to be either in between pessimistic and optimistic models, or greater than an optimistic one, was previously observed in Oto measurements [15]. Lastly, we observe that the pessimistic model at 2 GHz predicts lower path loss than even the optimistic model at 28 GHz.

4.4 Impact of Tx and Rx Placement

Having many Oti scenarios allows us to develop a sense of the “average” wireless channel by considering many data points as a single ensemble. However, having multiple locations means that we can also isolate specific features of the Tx and Rx placements from our Oti scenarios to understand their potential impact.

4.4.1 Different Sides of an Elevated Subway Track. We observe differences not only between measurement locations, but also between individual sidewalks measured at a single location. A notable

example of this is shown for the JLG-N-W and JLG-N-E scenarios in Figures 6(a) and 6(b). An elevated subway track bisects the two sides of the street; the receiver was placed at **JLG** directly in-line with JLG-N-W; JLG-N-E is the sidewalk on the far side of the street which has significant blockage from the subway track.

Figure 6(a) shows a consistent 10 dB higher path loss for JLG-N-E over the distances measured. Furthermore, Figure 6(b) shows the median azimuth beamforming gain for JLG-E-E is degraded by a further 1.8 dB, for a total median beamforming gain loss of almost 6 dB. This result indicates that elevated subway tracks or similar structures add a significant amount of path loss and environmental scattering, and more generally demonstrate how an Oti scenario is still heavily dependent on the outdoor propagation environment.

4.4.2 Different Floors of the Same Building. As a typical building occupies more than one floor, it is useful to understand what effect, if any, the height of a user has on the wireless channel. We use the measurements from **TEA** where the Rx was placed on the second and third floors, such that the Rx is at the same distance along the street, only higher or lower in elevation. The indoor layout of the second and third floors where the Rx is placed is largely identical, meaning any observed difference will be due to the outdoors propagation environment. The Tx was then placed along identical locations on the street sidewalks. The results of this comparison can be seen in Figures 6(c) and 6(d), which show that the third floor placement of the Rx experiences an 8–10 dB lower path loss than the second floor placement.

We observe that the street sidewalks along **TEA** have trees planted at regular intervals. Therefore, a plausible explanation for this result is that the higher floor has a view of the Tx which experiences less blockage due to foliage. We also note that the azimuth beamforming gain degradation is around 1 dB lower for the third floor. A lower blockage from foliage would also explain this effect, as foliage can create significant scattering [14, 41].

4.4.3 Angle of Incidence. As shown in [33], the AoI into the window can have an over 10 dB impact on the amount of loss experienced by the 28 GHz signal. Therefore, we may observe a widespread impact of the AoI into the glass on the measured path loss. In each

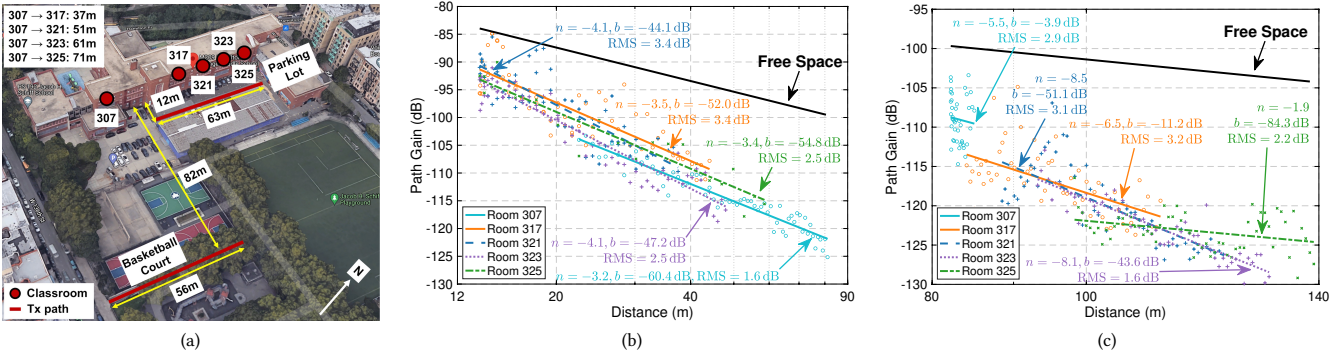


Figure 7: Summary of path gain measurements taken at HMS. (a) Map of measurement locations. Maroon lines represent paths along which the channel sounder Tx was moved for each classroom Rx location, which correspond to entries in Table 3. (b), (c) Per-classroom path gain models with the Tx placed along (b) the parking lot directly outside the classrooms and (c) the basketball court. Distances represent the three-dimensional Euclidean distance between Tx and Rx.

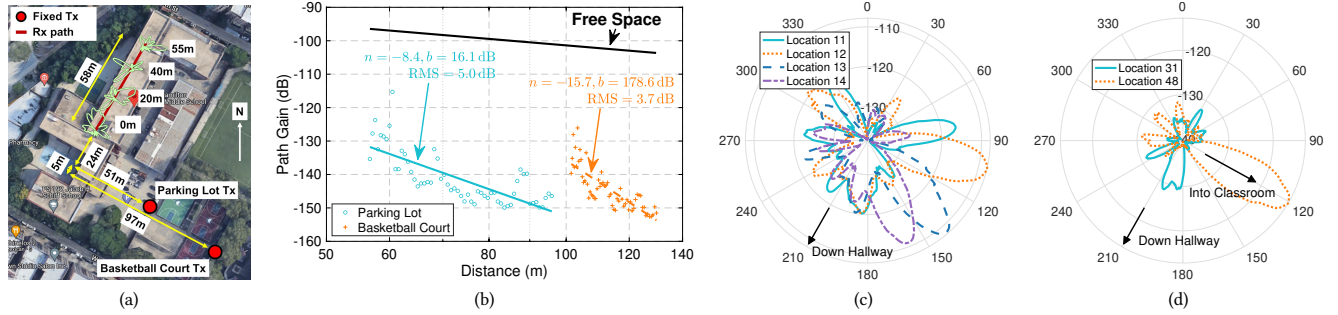


Figure 8: Hallway measurements at HMS taken from two different Tx locations. (a) Map of the hallway measurements and example power angular spectra for the Tx located in the parking lot. (b) Path gain models for both Tx locations. (c) Successive angular spectra showing the peak angle rotating as the Rx moves past a classroom door, demonstrating the presence of a strong propagation path via the nearest classroom. (d) Two other angular spectra showing two different dominant propagation paths; one through a classroom, and one down the hallway.

OtI scenario, the Tx is moved perpendicular/parallel to the window by the Rx, leading to a normal/oblique AoI into the window. The Tx was moved in both ways during the measurements at NWC. We cluster the NWC OtI scenarios according to the measurable street geometry by considering what AoI the straight line between the Tx and Rx has on the window glass. We generate two clusters, one where $\text{AoI} < 45^\circ$, and the second where $\text{AoI} \geq 45^\circ$. For cases where LOS from Tx to Rx is blocked, the real AoI for the mmWave signal is difficult to determine. Hence we do not include NWC-N-E or NWC-W-S as they lose LOS to NWC as the Tx moves farther away.

We observe a 9 dB difference between the two clusters at 50 m in Figure 6(e), close to the observed 10 dB range of glass transmission loss. We also observe that the difference between the two clusters becomes smaller at greater distances; this is an expected result as the path loss is prone to other effects at longer range. The azimuth beamforming plot in Figure 6(f) shows that the median beamforming gain is around 1 dB lower for the higher AoI group, implying that OtI scenarios with a larger AoI experience not only a greater path loss but also a larger degree of environmental scattering.

5 CASE STUDY: A PUBLIC SCHOOL

As **HMS** uses traditional glass for its windows, it experiences a significantly lower path loss compared to the other measured locations. Furthermore, **HMS** is a representative example of a public school building located within an NYC neighborhood with comparatively low Internet access. These two characteristics make **HMS** a location of particular interest. We analyze the measurements at **HMS** in classrooms which are mapped in Figure 7(a) and enumerated in

Table 3, and a hallway mapped in Figure 8(a). We then compare path gain models for the individual classrooms and study how the mmWave signal propagates into the indoor hallway. The dataset covering **HMS** is publicly available at [32].

5.1 Classroom Measurements

Measurements at **HMS** were taken with the Rx located in five classrooms along the third floor of the school building. We note that the classrooms are all very regular in dimension as well as interior layout. The Tx was moved along two paths, one along the school parking lot located directly outside the classrooms, and the other along the basketball courts located at a greater distance. A map of the school and measurement locations, along with path gain results for the two Tx paths, are shown in Figure 7.

The fitted models for the measurements with the Tx located in the parking lot in Figure 7(b) show a high degree of similarity, with similar fitted slopes close to $n = 4$, in line with the theoretical model developed in [42] for outdoor-to-indoor propagation at oblique incidence angles. The measured path gain values from different classrooms largely overlap, an understandable result given the uniformity of the five classrooms considered. The relatively low 10–20 dB excess loss above free space in Figure 4(a) indicates a strong potential for OtI coverage.

Similar results with the Tx located in the basketball court are shown in Figure 7(c). Unlike the measurements with the Tx in the parking lot, there is some dependence on the classroom being measured. In particular, Room 307 has a noticeably higher path gain compared to the other classrooms. One possible reason is the row

of trees visible near the middle of the map in Figure 7(a). As seen from ground level at the basketball court, these trees did partially block the view of the windows for classrooms 317 to 325, which likely accounts for the higher loss experienced by these classrooms.

5.2 Hallway Measurements

We also conducted measurements by moving the Rx along an interior hallway located behind the row of classrooms indicated in Figure 8(a). The Tx was kept in two fixed positions, one in the parking lot and the other at the basketball court, noted by the “Fixed Tx” locations in the same figure. The Rx was moved along the hallway in an identical manner for both Tx locations, leading to a total of 116 measurements taken of the interior hallway. The path gain and azimuth beamforming gain measurements are shown in Figure 8.

The path gain results in Figure 8(b) show a 5 dB difference between the two models, with the large n indicating a fast drop-off in received power as the Rx moves down the hallway. The plotted distance in Figure 8(b) is the three-dimensional Euclidean distance from Rx to Tx; the Rx was moved along a 58 m linear distance down the hallway in both measurements. This distance is compressed within the three-dimensional Euclidean distance, creating the particularly steep slopes. There was no direct line-of-sight path from Tx to Rx. Indoor locations far from a window typically have several candidate propagation paths [43]. In the case of these hallway measurements, we consider two likely methods [42]: (i) via the room most normal to the Tx, and (ii) via the room closest to the location of the Rx. We study the propagation mechanism by investigating the angular spectra $\bar{S}(d, \phi)$ measured at several Tx-Rx links.

Figure 8(a) shows angular spectra for different Rx locations along the hallway. There is no clear trend in the direction of the peak angles, lacking a persistent dominant direction along the hallway which would be characteristic of propagation method (i). Figure 8(c) shows how the peak angle rotates as the Rx moves past the doorway of Room 317, where locations {11, 12} and {13, 14} are locations on either side of the doorway. It is clear that the dominant method is (ii) and the Rx is receiving a signal through the doorway of Room 317; the rotating peak effect was observed for Rx locations close to other classroom doors as well.

The angular spectra in Figure 8(d) show that there are some Rx locations which receive a signal peak from Room 307 down the hallway, the room most normal to the Tx. This represents propagation method (i), and so we find that both propagation methods are active in this OI scenario, though method (ii) seems to be dominant.

6 MULTI-USER SUPPORT POTENTIAL

The support of multiple users with multiple beams is important for mmWave MIMO systems. We consider two OI scenarios at TEA described in Table 4 with the Tx and Rx reversed to study feasibility of OI multi-user MIMO. The Rx emulates a BS and measures from which directions the signal is received from the indoor Tx. The Tx was moved between four different rooms at TEA and the Rx was placed on outdoor balconies at the street corner and mid-way along the street, as shown in Figure 9(a).

The power angular spectra $\bar{S}(d, \phi)$ also shown in Figure 9(a) rotate as the Tx moves between rooms. Should this rotation be significant, the beams from different rooms will not overlap, allowing

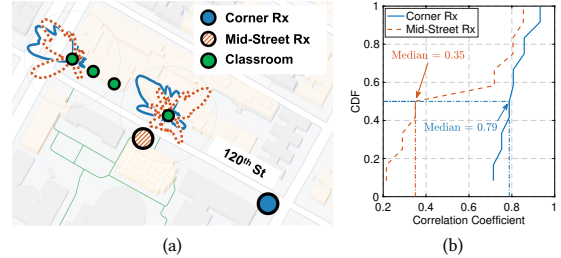


Figure 9: Measurements at TEA with Tx and Rx reversed. (a) Map of Rx locations on the balcony and angular spectra overlaid on select Tx locations. (b) CDF of correlation coefficient between power angular spectra.

for simultaneous coverage from the BS. To evaluate this effect, we compute the cross-correlation of $\bar{S}(d, \phi)$ across all pairs of rooms without repetition. In this context, the cross-correlation may be understood as a measure of the inter-user interference (IUI).

CDFs showing the distribution of $\bar{S}(d, \phi)$ cross-correlations for the two Rx locations are shown in Figure 9(b). The CDF for the corner Rx location shows a high median correlation coefficient of 0.79, likely caused by the similar oblique incidence angles for the rooms located at the far end of the street. This indicates a high level of IUI. The mid-street Rx location has a much lower median correlation coefficient of 0.35, indicating lesser IUI, which is likely due to the larger angular separation between Tx locations. Since high IUI suggests a diminished multi-user MIMO capability, these results indicate that a BS placed at a street corner, which is excellent for street canyon coverage, may struggle to simultaneously serve multiple users at the far end of the street with multiple beams.

7 GLASS-DEPENDENT OTI DATA RATES

The models in Section 4.3 are now used to develop a measure of link rate coverage for OI scenarios with “traditional” or Low-e glass. Table 5 defines typical parameters for the 28 GHz BS and UE representative of recent advances in state-of-the art mmWave hardware [44–48]. We select conservative values for these parameters to reduce the possibility of overestimating data rates, and we include an additional 5 dB of losses in NF. The resulting Rx noise floor is $N = -174 + 10 \log_{10} B + NF = -76$ dBm. In this analysis, we assume that the BS and UE are able to efficiently align their transmit and receive beams [49].

As the signal-to-noise (SNR) will determine the achievable data rate, we present a relevant measure of data rate coverage by considering the 10th percentile SNR(d), $SNR_{10}(d)$, which defines the SNR that 90% of users will exceed. The SNR in dB may be computed as $SNR(d) = P_{Tx} + G_{Tx} + G_{LNA} + G_{Rx} - G_{deg}(d) + G_{path}(d) - N$, where $G_{path}(d)$ is computed from our path gain model and $G_{deg}(d)$ is computed from the median azimuth beamforming gain.

By using an empirical path gain model M , we can represent the SNR as a normally distributed random variable $SNR \sim \mu(M) + \sigma(M) \cdot \mathcal{N}(0, 1)$, where μ and σ are the mean and standard deviation of M , respectively. M is itself a function of d , therefore a normally distributed SNR random variable is defined for every distance d .

We consider three SNR boundaries: 25 dB, 14 dB, and 4 dB. These represent minimum SNRs at which 256QAM 4/5, 16QAM 1/2, and QPSK 3/10 modulation and coding schemes (MCS) become advantageous to use. [50–52]. We can estimate link rates using an impaired Shannon capacity $\hat{D} = \rho \beta B \log_2(1 + 10^{(SNR-C)/10})$, where $\rho = 0.6$

Table 5: Typical device parameters for a 28 GHz Tx (BS) and Rx (UE)

Quantity	Symbol	Value	Ref.
Tx Power	P_{TX}	+28 dBm	[44]
Tx Antenna Gain	G_{TX}	23 dBi	[44]
Rx LNA Gain	G_{LNA}	13 dB	[45]
Rx Antenna Gain	G_{RX}	9 dBi	[46]
Rx Noise Figure	NF	4 + 5 dB	[47]
Bandwidth	B	800 MHz	[44, 48]

is the overhead factor, $\beta = 0.8$ is the time-division duplexing down-link ratio, and $C = 3$ dB is implementation loss. This leads to link rates of at least 2.8, 1.4, and 0.4 Gb/s for 256QAM, 16QAM, and QPSK respectively, close to values from 3GPP [50, 51].

Buildings with Traditional Glass. As shown in Sections 4.3 and 5, buildings with “traditional” glass experience lower path loss, suggesting a strong potential for OI coverage at 28 GHz. From Figure 4(a), we set the slope $n = 3$, intercept $b = -59.8$ dB, and $\sigma = 4.3$ dB. For each outdoor link distance $d \in \{10, 11, \dots, 200\}$, we compute the 10th percentile path gain given by the log-normal distribution $G_{path,i}(d) = b + n \cdot 10 \log_{10} d + \sigma \cdot N(0, 1)$. We also compute the median azimuth beamforming gain degradation $G_{deg,i} = 14.5 - G_{az,median}$ where $G_{az,median}$ is the median of the azimuth beamforming gain distribution for traditional glass in Figure 4(a) and 14.5 is the gain of the Rx antenna in azimuth.

The top curve in Figure 10 demonstrates $SNR_{10}(d) > 25$ dB for $d \leq 68$, meaning that 256-QAM modulation is supported for at least 90% of indoor users at a link distance of up to 68 m. This corresponds to $\hat{D} > 2.8$ Gb/s. 16-QAM 1/2 MCS for 90% of indoor users is supported up to 175 m, corresponding to $\hat{D} > 1.4$ Gb/s. These measurements covered a variety of Tx and Rx locations at **HMS** as shown in Figure 7(a), with many links occluded by foliage and with a large variation in the AoI. Thus, we believe these results to be representative of building constructions with traditional glass in typical urban environments. A 68 m link distance subtends 81° with a typical 10 m building standoff, which is within the beamsteering capability of phased array antennas suitable for outdoor BSes [44].

Buildings with Low-e Glass. We repeat the SNR calculations using the Low-e model in Figure 4(a), setting $n = 3$, $b = -79.6$ dB, and $\sigma = 8.4$ dB, producing the the lower curve of Figure 10. The results show that 256-QAM coverage cannot be supported for at least 90% of users even at the shortest realistic Tx-Rx link distance. Instead, 16-QAM 1/2 ($\hat{D} > 1.4$ Gb/s) and QPSK 3/10 ($\hat{D} > 0.5$ Gb/s) MCS may be supported up to 25 m and 49 m, respectively. As the Low-e glass model uses data from six distinct buildings, we believe this result is representative of buildings with Low-e glass.

The coverage experienced by an indoor UE has a large variation depending heavily on the window material. Indoor coverage potential is significantly higher for buildings with older, thinner glass. However, coverage at gigabit data rates is still feasible even in buildings with modern construction if BS is nearby (~20 m).

8 CONCLUSION

We addressed the lack of extensive OI mmWave measurements by conducting a large-scale measurement campaign consisting of over 2,000 Tx-Rx links across seven building sites in West Harlem, NYC. We used the measurements to develop models for OI path gain under various conditions. Among other things, these models show that data rates in excess of 2.8 Gb/s are achievable for at least 90% of indoor users in typical public school buildings with lightpole

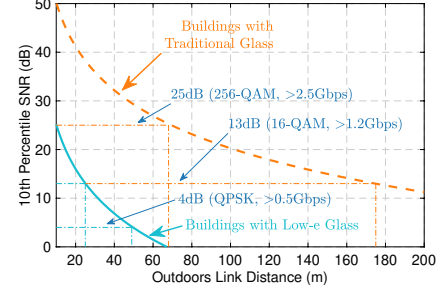


Figure 10: 10th percentile SNR predictions for buildings with Low-e or traditional glass windows, with coverage ranges d^* labelled for various MCS.

BS deployments at distances up to 68 m away. Rates in excess of 1.4 Gb/s can be achieved by a BS up to 175 m away. Similar light-pole deployments up to 49 m range are capable of providing data rates in excess of 400 Mb/s for users in buildings that use modern Low-e glass. As we expect the results to inform the deployment of mmWave networks in urban areas with low Internet access, thereby helping to improve connectivity and bridging the digital divide, the **HMS** public school dataset is made publicly available at [32].

While we show that high data rates in OI scenarios are achievable, we also show that OI multi-user support by a mmWave BS is challenging, with potentially high inter-user-interference. This illustrates the need for careful design of beamforming algorithms which take OI scenarios into account. We will study this in future work, supported by further measurement to ensure model accuracy. We will also use the 28 GHz phased array antenna modules integrated in the COSMOS Testbed [53] to implement and test the designed algorithms as well as take wideband channel measurements for other important results, such as the delay spread.

9 ACKNOWLEDGEMENTS

This work was supported by NSF grants CNS-1827923, CNS-2148128, OAC-2029295, and EEC-2133516, and NSF-BSF grant CNS-1910757. Rodolfo Feick’s work is supported by Chilean Research Agency grants PIA/APOYO AFB180002 and ANID/REDES 180144. We thank Angel Daniel Estigarribia, Zixiang Zheng, Carson Garland, and Shivan Mukherjee for their help with the measurements. We thank Basil Masood, Taylor Riccio, Jennifer Govan, and Barbara Han for their support during the measurement campaigns at Hamilton Grange, Miller Theatre, Teachers’ College, and Jerome L. Greene. We thank Tingjun Chen for his helpful suggestions.

REFERENCES

- [1] FCC. 2021. Notes from the FCC: Addressing the Homework Gap. <https://www.fcc.gov/news-events/notes/2021/02/01/addressing-homework-gap>. (2021).
- [2] NYC Mayor’s Office of the CTO. 2020. The New York City Internet Master Plan. https://www1.nyc.gov/assets/cto/downloads/internet-master-plan/NYC_IMP_1.7.20_FINAL-2.pdf. (2020).
- [3] M. Polese, F. Restuccia, and T. Melodia. 2021. DeepBeam: Deep Waveform Learning for Coordination-Free Beam Management in MmWave Networks. In *Proc. ACM MobiHoc*.
- [4] Z. L. Fazliu, C. F. Chiasserini, F. Malandrino, and A. Nordio. 2020. Graph-Based Model for Beam Management in Mmwave Vehicular Networks. In *Proc. ACM MobiHoc*.
- [5] S. G. Sanchez, S. Mohanti, D. Jaisinghami, and K. R. Chowdhury. 2022. Millimeter-Wave Base Stations in the Sky: An Experimental Study of UAV-to-Ground Communications. *IEEE Trans. Mobile Comput.*, 21, 2, 644–662.
- [6] S. Aggarwal, U. S. Sardesai, V. Sinha, D. D. Mohan, M. Ghoshal, and D. Koutsoukolas. 2020. LiBRA: Learning-Based Link Adaptation Leveraging PHY Layer Information in 60 GHz WLANs. In *Proc. ACM CoNEXT*.

- [7] Z. He, S. Mao, S. Kompella, and A. Swami. 2017. On Link Scheduling in Dual-Hop 60-GHz mmWave Networks. *IEEE Trans. Veh. Technol.*, 66, 12, 11180–11192.
- [8] D. Chizhik, J. Du, R. Feick, M. Rodriguez, G. Castro, and R. A. Valenzuela. 2020. Path Loss and Directional Gain Measurements at 28 GHz for Non-Line-of-Sight Coverage of Indoors With Corridors. *IEEE Trans. Antennas Propag.*, 68, 6, 4820–4830.
- [9] V. Raghavan, A. Partyka, A. Sampath, S. Subramanian, O. H. Koymen, K. Ravid, J. Cezanne, K. Mukkavilli, and J. Li. 2018. Millimeter-Wave MIMO Prototype: Measurements and Experimental Results. *IEEE Commun. Mag.*, 56, 1, 202–209.
- [10] K. Du, O. Ozdemir, F. Erden, and I. Guvenç. 2021. 28 GHz Indoor and Outdoor Propagation Measurements and Analysis at a Regional Airport. In *Proc. IEEE PIMRC*.
- [11] S. Y. Jun, D. Caudill, J. Chuang, P. B. Papazian, A. Bodí, C. Gentile, J. Senic, and N. Golmie. 2020. Penetration Loss at 60 GHz for Indoor-to-Indoor and Outdoor-to-Indoor Mobile Scenarios. In *Proc. EuCAP*.
- [12] H. Zhao, R. Mayzus, S. Sun, M. Samimi, J. K. Schulz, Y. Azar, K. Wang, G. N. Wong, F. Gutierrez, and T. S. Rappaport. 2013. 28 GHz Millimeter Wave Cellular Communication Measurements for Reflection and Penetration Loss In and Around Buildings in New York City. In *Proc. IEEE ICC*.
- [13] M. Z. Aslam, Y. Corre, J. Belschner, G. S. Arockiaraj, and M. Jager. 2020. Analysis of 60-GHz In-street Backhaul Channel Measurements and LiDAR Ray-based Simulations. In *Proc. EuCAP*.
- [14] J. Du, D. Chizhik, R. Feick, M. Rodriguez, G. Castro, and R. A. Valenzuela. 2020. Suburban Fixed Wireless Access Channel Measurements and Models at 28 GHz for 90% Outdoor Coverage. *IEEE Trans. Antennas Propag.*, 68, 1, 411–420.
- [15] T. Chen, M. Kohli, T. Dai, A. D. Estigarribia, D. Chizhik, J. Du, R. Feick, R. A. Valenzuela, and G. Zussman. 2019. 28 GHz Channel Measurements in the COSMOS Testbed Deployment Area. In *Proc. ACM mmNets'19 Workshop*.
- [16] Y. Xing and T. S. Rappaport. 2018. Propagation Measurement System and Approach at 140 GHz-Moving to 6G and Above 100 GHz. In *Proc. IEEE GLOBECOM*.
- [17] J. Ko, Y.-J. Cho, S. Hur, T. Kim, J. Park, A. F. Molisch, K. Haneda, M. Peter, D.-J. Park, and D.-H. Cho. 2017. Millimeter-Wave Channel Measurements and Analysis for Statistical Spatial Channel Model in In-Building and Urban Environments at 28 GHz. *IEEE Trans. Wireless Commun.*, 16, 9, 5853–5868.
- [18] K. Du, O. Mujumdar, O. Ozdemir, E. Ozturk, I. Guvenç, M. L. Sichitiu, H. Dai, and A. Bhuyan. 2022. 60 GHz Outdoor Propagation Measurements and Analysis Using Facebook Terragraph Radios. In *Proc. IEEE RWS*.
- [19] M. Samimi, K. Wang, Y. Azar, G. N. Wong, R. Mayzus, H. Zhao, J. K. Schulz, S. Sun, F. Gutierrez, and T. S. Rappaport. 2013. 28 GHz Angle of Arrival and Angle of Departure Analysis for Outdoor Cellular Communications Using Steerable Beam Antennas in New York City. In *Proc. IEEE VTC*.
- [20] A. Shkel, A. Mehramani, and J. Kusuma. 2021. A Configurable 60GHz Phased Array Platform for Multi-Link mmWave Channel Characterization. In *Proc. IEEE ICC Workshops*.
- [21] Y. Xing and T. S. Rappaport. 2021. Millimeter Wave and Terahertz Urban Microcell Propagation Measurements and Models. *IEEE Commun. Lett.*, 25, 12, 3755–3759.
- [22] Y. Zhang, D. J. Love, N. Michelusi, J. V. Krogmeier, S. Jyoti, A. Sprintson, and C. R. Anderson. 2018. Improving Millimeter-wave Channel Models for Suburban Environments with Site-specific Geometric Features. In *Proc. ACES*.
- [23] A. Narayanan, E. Ramadan, J. Carpenter, Q. Liu, Y. Liu, F. Qian, and Z.-L. Zhang. 2020. A First Look at Commercial 5G Performance on Smartphones. In *Proc. ACM WWW*.
- [24] O. H. Koymen, A. Partyka, S. Subramanian, and J. Li. 2015. Indoor mm-Wave Channel Measurements: Comparative Study of 2.9 GHz and 29 GHz. In *Proc. IEEE GLOBECOM*.
- [25] NIST Communications Technology Laboratory. 2022. NextG Channel Model Alliance. (2022). <https://www.nist.gov/ctl/nextg-channel-model-alliance>.
- [26] C. A. L. Diakhate, J.-M. Conrat, J.-C. Cousin, and A. Sibille. 2017. Millimeter-wave Outdoor-to-Indoor Channel Measurements at 3, 10, 17 and 60 GHz. In *Proc. EuCAP*.
- [27] N. Netsetikas, N. Babu, M. H. Tariq, C. B. Papadias, J. Du, D. Chizhik, R. Valenzuela, M. Rodriguez, and R. Feick. 2022. 60 ghz outdoor to indoor (o2i) propagation measurements in a university campus. In *Proc. IEEE SPAWC Workshop*.
- [28] C. U. Bas, R. Wang, T. Choi, S. Hur, K. Whang, J. Park, J. Zhang, and A. F. Molisch. 2018. Outdoor to Indoor Penetration Loss at 28 GHz for Fixed Wireless Access. In *Proc. IEEE ICC*.
- [29] C. Larsson, F. Harrysson, B.-E. Olsson, and J.-E. Berg. 2014. An Outdoor-to-Indoor Propagation Scenario at 28 GHz. In *Proc. EuCAP*.
- [30] FCC. 2021. FCC Established Two New Innovation Zones in Boston and Raleigh. <https://www.fcc.gov/document/fcc-established-two-new-innovation-zones-boston-and-raleigh-0>. (2021).
- [31] D. Raychaudhuri, I. Seskar, G. Zussman, T. Korakis, D. Kilper, T. Chen, J. Kolodziejczyk, M. Sherman, Z. Kostic, X. Gu, H. Krishnaswamy, S. Maheshwari, P. Skrimponis, and C. Gutterman. 2020. Challenge: COSMOS: A City-Scale Programmable Testbed for Experimentation with Advanced Wireless. In *Proc. ACM MobiCom*.
- [32] M. Kohli, A. Adhikari, G. Avci, S. Brent, J. Moser, S. Hossain, A. Dash, I. Kadota, R. Feick, D. Chizhik, J. Du, R. A. Valenzuela, and G. Zussman. 2022. 28GHz Outdoor-Indoor West Harlem NYC Public School Dataset. (2022). <https://nextg.nist.gov/submissions/131>.
- [33] M. Kohli, A. Adhikari, G. Avci, S. Brent, A. Dash, J. Moser, S. Hossain, I. Kadota, C. Garland, S. Mukherjee, R. Feick, D. Chizhik, J. Du, R. A. Valenzuela, and G. Zussman. 2022. Outdoor-to-Indoor 28 GHz Wireless Measurements in Manhattan: Path Loss, Environmental Effects, and 90% Coverage. (2022). arXiv: 2205.09436 [eess.SP]. <https://arxiv.org/abs/2205.09436>.
- [34] M. Schmieder, M. Peter, R. Askar, I. Komsic, and W. Keusgen. 2018. Measurement and Characterization of 28 GHz High-Speed Train Backhaul Channels in Rural Propagation Scenarios. In *Proc. EuCAP*.
- [35] NYC Dept of Information Technology & Telecommunications. 2022. 5G Rollout. (2022). <https://www1.nyc.gov/site/doitt/business/5g-design/5g.page>.
- [36] Samsung. 2022. Compact Macro (Access Unit). (2022). <https://www.samsung.com/global/business/networks/products/radio-access/access-unit/>.
- [37] K. Du, O. Ozdemir, F. Erden, and I. Guvenç. 2021. Sub-Terahertz and mmWave Penetration Loss Measurements for Indoor Environments. In *Proc. IEEE ICC Workshops*.
- [38] H. Kim and S. Nam. 2021. Transmission Enhancement Methods for Low-Emissivity Glass at 5G mmWave Band. *IEEE Antennas Wireless Propag. Lett.*, 20, 1, 108–112.
- [39] C. Vargas, L. da Silva Mello, and R. C. Rodriguez. 2017. Measurements of Construction Materials Penetration Losses at Frequencies From 26.5 GHz to 40 GHz. In *Proc. IEEE PACRIM*.
- [40] 3GPP. 2020. Study on Channel Model for Frequencies From 0.5 to 100 GHz (3GPP TR 38.901 version 16.1.0 Release 16). (2020). https://www.etsi.org/deliver/etsi_tr/138900_138999/138901/16.01.00_60/tr_138901v160100p.pdf.
- [41] S. Yang, J. Zhang, and J. Zhang. 2019. Impact of Foliage on Urban MmWave Wireless Propagation Channel: A Ray-tracing Based Analysis. In *Proc. IEEE ISAP*.
- [42] D. Chizhik, J. Du, and R. A. Valenzuela. 2021. Universal Path Gain Laws for Common Wireless Communication Environments. *IEEE Trans. Antennas Propag.*.
- [43] D. Shakya, D. Chizhik, J. Du, R. A. Valenzuela, and T. S. Rappaport. 2022. Dense Urban Outdoor-Indoor Coverage from 3.5 to 28 GHz. In *Proc. IEEE ICC*.
- [44] B. Sadhu, Y. Tousi, J. Hallin, S. Sahl, S. K. Reynolds, O. Renstrom, K. Sjogren, O. Haapalahti, N. Mazor, B. Bokinge, G. Weibull, H. Bengtsson, A. Carlinger, E. Westesson, J.-E. Thillberg, L. Rexberg, M. Yeck, X. Gu, M. Ferriss, D. Liu, D. Friedman, and A. Valdes-Garcia. 2017. A 28-GHz 32-Element TRX Phased-Array IC With Concurrent Dual-Polarized Operation and Orthogonal Phase and Gain Control for 5G Communications. *IEEE J. Solid-State Circuits*, 52, 12, 3373–3391.
- [45] Z. Deng, J. Zhou, H. J. Qian, and X. Luo. 2021. A 22.9-38.2-GHz Dual-Path Noise-Cancelling LNA With 2.65-4.62-dB NF in 28-nm CMOS. *IEEE J. Solid-State Circuits*, 56, 11, 3348–3359.
- [46] I.-J. Hwang, J.-I. Oh, H.-W. Jo, K.-S. Kim, J.-W. Yu, and D.-J. Lee. 2021. 28/38 GHz Dual-Band Vertically Stacked Dipole Antennas on Flexible Liquid Crystal Polymer Substrates for Millimeter-Wave 5G Cellular Handsets. *IEEE Trans. Antennas Propag.*.
- [47] A. Ersjadi, S. Palermo, and K. Entesari. 2021. A 22.2-43 GHz Gate-Drain Mutually Induced Feedback Low Noise Amplifier in 28-nm CMOS. In *Proc. IEEE RFIC*.
- [48] Y.-W. Chang, T.-C. Tsai, J.-Y. Zhong, J.-H. Tsai, and T.-W. Huang. 2020. A 28 GHz Linear and Efficient Power Amplifier Supporting Wideband OFDM for 5G in 28nm CMOS. In *Proc. IEEE/MTT-S IMS*.
- [49] M. S. Zia, D. M. Blough, and M. A. Weitnauer. 2022. Effects of SNR-Dependent Beam Alignment Errors on Millimeter-Wave Cellular Networks. *IEEE Trans. Veh. Technol.*.
- [50] ATIS 3GPP. 2020. Study on Support of NR Downlink 256 Quadrature Amplitude Modulation (QAM) for Frequency Range 2 (FR2) (ATIS.3GPP.38.883.V1600). (2020). <https://www.atis.org/wp-content/uploads/3gpp-documents/Rel16/ATIS.3GPP.38.883.V1600.pdf>.
- [51] 3GPP. 2019. User Equipment (UE) Conformance Specification; Radio Transmission and Reception (3GPP TS 38.521-4 version 15.0.0 Release 15). (2019). https://www.etsi.org/deliver/etsi_ts/138500_138599/13852104/15.00.00_60_ts_13852104v150000p.pdf.
- [52] E. Perala, T. Levanen, T. Ihälainen, S. Nielsen, M. H. Ng, M. Renfors, and M. Valkama. 2018. 5G New Radio Base-Station Sensitivity and Performance. In *ISWCS*.
- [53] T. Chen, P. Maddala, P. Skrimponis, J. Kolodziejczyk, X. Gu, A. Paidimarri, S. Rangan, G. Zussman, and I. Seskar. 2022. Programmable and Open-Access Millimeter-Wave Radios in the PAWR COSMOS Testbed. In *Proc. ACM MobiCom'21 WiNTECH Workshop*.